AN EMPIRICAL MODEL OF HIGH SPATIAL AND TEMPORAL RESOLUTION FOR RADAR RAINFALL NOWCASTING

J1.1

Nazario D. Ramirez-Beltran*
University of Puerto Rico, Mayagüez, PR

Luz Torres Molina
University of Puerto Rico, Mayagüez, PR

Joan M. Castro
University of Puerto Rico, Mayagüez, PR

Sandra Cruz-Pol
University of Puerto Rico, Mayagüez, PR

José G. Colom-Ustáriz
University of Puerto Rico, Mayagüez, PR

Nathan Hosannah
University of Puerto Rico, Mayagüez, PR

1. INTRODUCTION

Rainfall nowcasting algorithm for convective storms is introduced in this work. The algorithm uses high resolution radar data to forecasts the evolving distribution of rainfall rate. It is assumed that for a short time period, a rain cloud behaves as a rigid object, with all parts moving in the same direction at a constant speed. Thus, the most likely future rainfall areas are estimated by tracking rain cell centroid advection in consecutive radar images. To estimate the growth or decay of rainfall intensity, a nonlinear regression model varying in the time and space domain is proposed to predict the most likely rainfall rate. This rainfall nowcasting algorithm was validated against five rainfall events which occurred over western Puerto Rico. Results show that the nowcasting algorithm is a potential tool to couple with a hydrological numerical model to forecast inundation areas.

Inundation and flash floods are occurring more frequently not only in tropical areas, but also in different climate conditions around the world (Burroughs, 2001). The impacts on human/ animal mortality and on the economy are one of the most important natural hazards that are frequently monitored. Puerto Rico is heavily affected by rainfall due to warm-cloud top convective processes that are induced by local sea breeze- and/or orographic features and during the summer by tropical storms and during the winter by cold fronts. A ceilometer shows that some of the local convective storms developed in the western part of Puerto Rico are below 3 km; i.e., some storms are missed because NEXRAD radar is located about 104 km away from the studied area and reflectivity is measured at about 3 km above the surface due to mountains. The uses of a radar network with high resolution and covering NEXRAD missing areas are important for flood forecasting efforts, and for understanding hydro meteorological processes. This current work represents the first time that a high resolution radar technology is used for rainfall forecasting in the western part of Puerto Rico.

Recently, the National Oceanic and Atmospheric Administration, and the National Weather Service (NOAA/NWS) has pointed out that in a near-term forecast period the numerical weather prediction models currently have lesser precipitation forecast skills than extrapolation of current radar rainfall observations (http://www.nws.noaa.gov/oh/hrl/hag/empe_mpn/). There are some authors that also support this idea (Van Horne, 2003; Wilson 2004; Thorndahl, et al. 2010). Extrapolation techniques are usually conducted by using statistical methods which have been developed during the last four decades. Rodríguez-Iturbe et al. (1984; 1987) proposed a stochastic model for forecasting rainfall in which storms arrive in a Poisson

Corresponding author Nazario D. Ramirez-Beltran, Industrial Engineering, University of Puerto Rico, Mayaguez, P.R. 00680, Nazario.ramirez@upr.edu

process at a single site. Each storm in the Poisson process consists of a cluster of random number of rain cells, with each cell having random duration and intensity. Cowpertwait et al. (2007) suggested a conceptual stochastic model in which storm origins occur in the Poisson process, with each storm having a random lifetime. Although the point process is theoretically attractive for a single site, it becomes cumbersome for computing the rainfall rate at each pixel of a radar field.

Dixon and Weiner (1993) developed a system for identifying and tracking convective storms. The algorithm essentially performs three major tasks: identification of convective storms, tracking storms, and predicting some storm parameters. The identification of convective cells is based on identify the contiguous rain pixels that satisfying reflectivity intensity and volume thresholds. The selected threshold, were $z \geq 35\,dBz$ and $V \geq 50\,km^3$, for reflectivity and volume, respectively. The tracking system is based on minimizing the distance and the difference in volume among all possible paths for a given storm. The optimization problem reduces to solving the assigning problem, which is usually solved by using the Hungarian method. The forecast method is based on a double exponential smoothing model (Abraham and Ledolter, 1983). The storm parameters that were forecasted are the centroid, reflectivity volume, and the parameters of an ellipse, since it was assumed that the projected reflectivity approaches to an elliptical form. The major challenge was encountered when forecasting the centroids of a storm that splits or merges, and when these events occurred, the algorithm made an incorrect forecast. To fix this, the algorithm was fed with information about when a storm was splitting, allowing for new tracking histories to start, and if a merge occurred, the history of some storms could disappear. They used a lead time that varied from 6 to 30 minutes with increment of 6 minutes, and found that forecast degradation occurred as soon as lead time increases.

In this study, we present a novel rainfall nowcasting model designed to work with high spatial and temporal resolution radar rainfall data. The selected radar provides coverage over the western area of Puerto Rico. The second section presents a description of the radar network and data used in this study. The third section describes the proposed algorithm to identify the rainfall cells and to estimate the cloud motion vector, which then is used to determine the most likely rain areas. A nonlinear regression model is also introduced in this section to represent the spatial and temporal rainfall variability. The fourth section shows validation results and the last section presents some conclusions and recommendations.

2. DATA

Puerto Rico is located in the northeastern Caribbean Sea and is one of the Greater Antilles islands. As mentioned before, precipitation is primarily affected by troughs imbedded in easterly waves during hurricane season (June-November), cold fronts during winter months (December-February), and local convective storms generated by sea breeze- and/or orographic features mostly occurred during the afternoon. Weather events are monitored using NEXRAD radar, a WSR-88D unit located in Cayey, Puerto Rico (18.12°N, 66.08°W, and 886.63 m elevation). The operating frequency is 2.7 GHz or 10 cm wavelength is free space (S-band). The maximum radial distance (horizontal range) is 462 km, and this radar scans the entire island every 6 minutes. In 2012, the first node of a 3-radar network (TropiNet) was setup in western Puerto Rico to complement the NEXRAD radar operation system and specifically to observe weather phenomena that occurs at the lowest 2 km of the troposphere. TropiNet will address the limitations of identifying boundary layer phenomena in this tropical environment, such as beam blockage and the Earth's curvature. TropiNet has three X-band dual-polarized Doppler weather radars with range resolution of 0.06 km and 1 min temporal scan resolution (Galvez, et al., 2009; 2013). Radars were setup at three locations in west Puerto Rico, including Isabela, Lajas, and Cabo Rojo, all with a 40 km radial coverage.

Corresponding author Nazario D. Ramirez-Beltran, Industrial Engineering, University of Puerto Rico, Mayaguez, P.R. 00680, Nazario.ramirez@upr.edu

Data used in this extended abstract were collected from the TropiNet unit located in Cabo Rojo, Puerto Rico (18.16°N, 67.17°W, and at 65 m of elevation). The working frequency is 9.41 GHz ± 30 MHz (3.19 cm wavelength in free space). Data were collected at 3 degrees elevation over the horizontal plane. Although radar scan is obtained every minute, the instantaneous reflectivities observed every 10 minutes were the inputs to the rainfall nowcasting algorithm. Data used for developing and validating the rainfall nowcasting algorithm include five convective storms that occurred in western Puerto Rico between March and October 2012 and during February 2014. The duration of these rainfall events varies from 5 to 7 hours with an average of 6 hours. The total number of raining hours during these five storms was 30. Table 1 describes the studied storms.

Table 1. Characteristics of studied storms.

Date	Duration (UTC)	Storm Type	Storm Impacts
March 28, 2012	7 hr. 16:27-23:58	Stationary trough	Impacts rivers, water on the road, and significant rainfall accumulation
March 29, 2012	6 hr. 00:36-06:53	Stationary trough	Impacts rivers, water on the road, significant rainfall accumulation
April 30, 2012	5 hr. 17:55-22:21	Convective storm	Numerous showers over western Puerto Rico at the afternoon
October 10, 2012	5 hr. 16:10-21:43	Convective storm	Some urban flooding
February 12, 2014	7 hr. 16:00-23:29	Heavy convective storm	Reduced visibilities and ponding of water on roadways and low lying areas

3. METHODOLOGY

A warm-cloud rainfall event is the result of a complex thermodynamic process that starts with the nucleation of cloud drops, continues with drop growth, and concludes with water drop precipitation. This process may last a few minutes or a few hours depending of the atmospheric conditions (Houze 1993). Thus, the introduced algorithm uses a sequence of radar rainfall data to estimate the rainfall field by first predicting the most likely rainfall areas and then predicting the expected rainfall rate in each rain pixel. An empirical model is built to represent the rainfall process; thus, it is important to identify the variables that are related to the precipitation process. The suggested regression model is developed under the following assumptions:

- It is expected that in a short time period (~10 min) a rain cloud behaves approximately as a rigid object and the cloud rain pixels moves in a constant speed and direction. Thus, the most likely future rainfall areas can be estimated by using the advection of centroids of rain cells in consecutive images.
- The current radar reflectivity is a function of the previous reflectivity images observed in surrounding areas centered on the location of a predicted pixel, and also is a function of the ratio of reflectivity of a pixel to reflectivity of the cell convective core.

The postulated rainfall nowcasting algorithm involves two major tasks: 1) predicting the future location of the rain pixels, and 2) predicting rainfall rate at each pixel.

3.1 Estimation of future rainfall areas

Estimation of the most likely rain fields requires estimation of the cloud motion vector, which was introduced in a previous publication (Ramirez-Beltran, et al., 2015). Here a brief description is presented. A threshold is used to identify pixel having rainfall; for instance, all the pixels that exhibit reflectivity larger than 20 dBz are selected in a given radar image. The identification of contiguous rain pixels is determined by searching through the rows and columns of the last two radar images for values that satisfy the reflectivity threshold and also having either three contiguous rows or columns with no rain. The contiguous rain pixels that satisfy the reflectivity threshold will be called rain cells.

Let assume that the last two radar images exhibit a single rain cell observed at two different instant in time; for a more general case a combinatory linear optimization problem is solved (Dixon and Weiner 1993). Thus, two consecutive centroids of a rainfall cell were

Corresponding author Nazario D. Ramirez-Beltran, Industrial Engineering, University of Puerto Rico, Mayaguez, P.R. 00680, Nazario.ramirez@upr.edu

computed to estimate the displacement of the cloud cell. Let $C_{t-1}(x_{t-1}, y_{t-1})$ and $C_t(x_t, y_t)$ be the centroids of a rain cell at time $t-1$ and t, respectively. The meridional and zonal displacement between two consecutives centroids is estimated as follows:

$$\Delta x = x_t - x_{t-1} \quad \text{and} \quad \Delta y = y_t - y_{t-1} \qquad (1)$$

Thus, using elementary trigonometry functions the modulus and direction of the motion vector is estimated. Finally, the motion vector is used to predict the location of the rain pixels. Let $P_t(i,j)$ and $P_{t+1}(i,j)$ be matrices indicating the locations of all rain pixels of the *P* rain cell at time t and $t+1$, respectively. Thus, each pixel of the *P* cell is added to the corresponding centroid displacement to estimate the future locations of the rain pixels, and expressed as follows:

$$P_{t+1}(k,l) = P_t(i + \Delta x, j + \Delta y) \qquad (2)$$

Figure 1 shows the motion vector and the most likely rainy areas. Prediction was computed with 30 minutes lead time. The top panel shows the observed rain areas and the bottom panel shows the forecasts rainfall area.

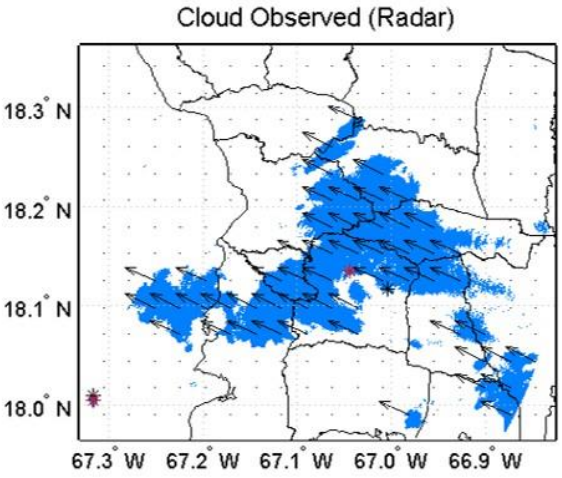

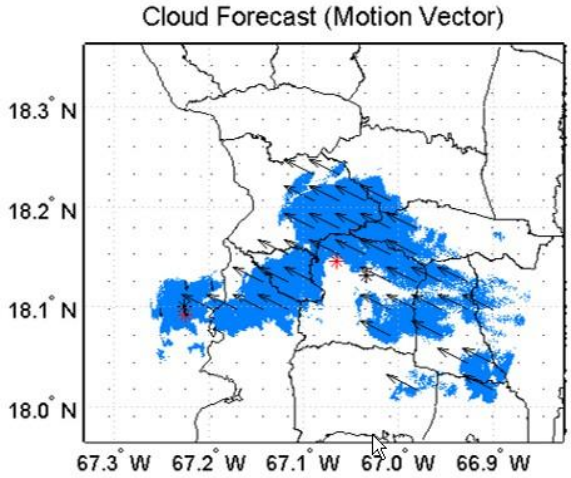

Figure 1. Predicting rainfall area for a storm that occurred on Puerto Rico March 28, 2012 1840 UTC; upper panel is the observed values and the bottom panel is the forecast.

3.2 Predicting rainfall rate

The rainfall process exhibits significant changes in time and space, and it can be characterized as a non-stationary stochastic process. To face the non-stationary characteristic of the process, parameters are estimated at each time and spatial domain. Thus, the dynamic changes on the mean are inherent in the time and space domains of the model. The stochastic characteristics of the process are represented by a nonlinear time and spatial lag model, which is an approximation to a stochastic transfer function model (Ramirez-Beltran et al. 2008; Box and Jenkins, 1994). Estimation of rain rate at a given space and time requires consideration of cloud status at the current time and also at consecutive previous points in time as well as the influence of the motion vector; i.e., a model that depends only on current cloud conditions is an incomplete representation of the rainfall process because the rain rate at the current time is the result of the evolution of microphysical processes that started several minutes earlier while the wind vector determined the possible place where drops may arrive to the surface. Therefore, a reasonable model to represent the rain rate would be a nonlinear

Corresponding author Nazario D. Ramirez-Beltran, Industrial Engineering, University of Puerto Rico, Mayaguez, P.R. 00680, Nazario.ramirez@upr.edu

regression model. The studied area includes 740×940 pixels of 0.06 km grid size, and was divided in squares of $a \times a$ pixels, which will be called a window. Several window sizes were explored for $a = \{7, 9, 11, \ldots, 25\}$ and it was found that the larger the window size the larger the number of degree of freedom (df); however, resolution was degraded with increased window size. To derive a model for a high resolution with robust and consistent estimators, it was necessary to have more than 50 df, where df in a regression model is computed as follows: $df = a \times a - b$, which $a \times a$ is the total observations in a window and b is the number of parameters included in the model, in this case $b = 4$. Experimentally, it was found that the optimum window size was $a = 9$ since there is enough df to derive a regression model and acceptable resolution. Thus, the studied area includes at most 8,528 windows (82×104). When there are not enough data at time $t-1$ and/or at $t-2$, the Kriging interpolation method was used to estimate the rain pixels to derive the corresponding predictors (Wackernagel 2003). A stochastic nonlinear model that control the expected domain was inspired on a previous work (Ramirez-Beltran et al. 2008). An empirical model in time and space domain is proposed to predict rainfall variability and can be expressed as follows:

$$h_{t,k}(i,j) = \alpha_{t,k} + (\beta_{t,k} - \alpha_{t,k})\phi_{t,k}\{1 - e^{-[\delta_{1,t,k}\bar{h}_{t-1,k}(i,j) + \delta_{2,t,k}\bar{h}_{t-2,k}(i,j) + \delta_{3,t,k}m_{t-1,k}(i,j)]}\} + \varepsilon_{t,k}(i,j) \quad (3)$$

where

$$\delta_{i,t,k} \geq 0, \quad i = 1,2,3 \quad \text{and} \quad 0 < \phi_{t,k} \leq 1.1 \quad (4)$$

$$\bar{h}_{t-1,k}(i,j) = \frac{1}{\eta}\sum_{p\in A}\sum_{q\in A} h_{t-1,k}(i+p, j+q) \quad (5)$$

$$m_{t-1,k}(i,j) = \frac{\sum_{p\in A}\sum_{q\in A} h_{t-1,k}(i+p,j+q)}{\sum_{p\in A}\sum_{q\in A} h_{t-1}(i'+p,j'+q)} \quad (6)$$

$$A = \{0, \pm 1, \ldots, \pm s, \text{ and } s < a\} \quad (7)$$

where $h_{t,k}(i,j)$ is reflectivity observed at time t, in the window k, and in a pixel located at (i,j); $\bar{h}_{t-1,k}(i,j)$ is the average reflectivity variable observed at time $t-1$ and at location (i,j) used to explain reflectivity at time t, in window k; and η is the number of elements involved in the summation. The spatial lags p and q will take the values of $0, \pm 1, \ldots, \pm s$ and $s < a$. Several values of s were explored and the one that exhibited the largest correlation between the surrounding pixels in time $t-2$ and $t-1$ with the center pixel on time t was selected. In this particular case the best results were found when $s = 1$ (Figure 2a). $\beta_{t,k}$ and $\alpha_{t,k}$ are the maximum and the minimum observed reflectivities at time $t-2$ and $t-1$ in the window k; $m_{t-1,k}(i,j)$ is the ratio of observed reflectivity at a pixel to the maximum reflectivity of the rain cell at time $t-1$ and at window k (Figure 2b); where (i',j') is the location of the maximum reflectivity in a cell and (i,j) is the location of the predicted pixel at time $t-1$ of window k; $\phi, \text{and } \delta's$ are the regression parameters at the window k and are restricted to be positive or equal to zero. In addition the $\phi_{t,k}$ parameter, which is a bias correction factor is restricted to be less than or equal to 1.1; this threshold value were found by inspection. The random variable, $\varepsilon_{t,k}(i,j)$, is a sequence of an unobserved random variables with mean zero and constant variance associated to the pixel (i,j).

Reflectivity at a single pixel at the current time t is related to features from surrounding pixels located in the previous two radar images. Figure 2a) shows the schematic representation of predictors and the predicted pixel. Figure 2b) shows a graphical representation of convective core and the predicted pixel.

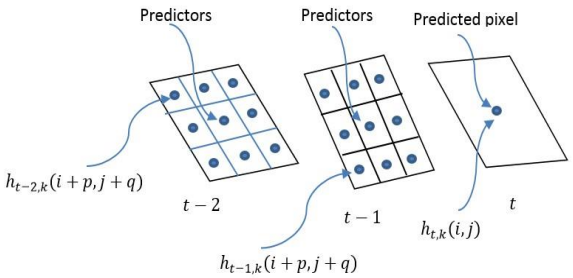

Figure 2a). Schematic representation of predictors and predicted pixels, for $s = 1$.

Corresponding author Nazario D. Ramirez-Beltran, Industrial Engineering, University of Puerto Rico, Mayaguez, P.R. 00680, Nazario.ramirez@upr.edu

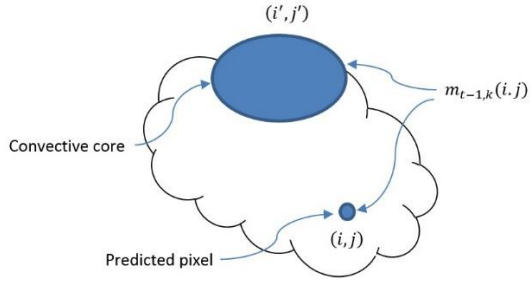

Figure 2b). A schematic representation of the convective core and a predicted pixel.

The proposed nowcasting algorithm includes a nonlinear regression model (Montgomery et. al., 2012); i.e., a well-planned approach is used to properly solve the nonlinear constrained problem. The introduced approach includes two steps: identifying the initial point, and using a constrained nonlinear optimization technique to estimate the final parameter set for each window (Ramirez-Beltran et al. 2008).

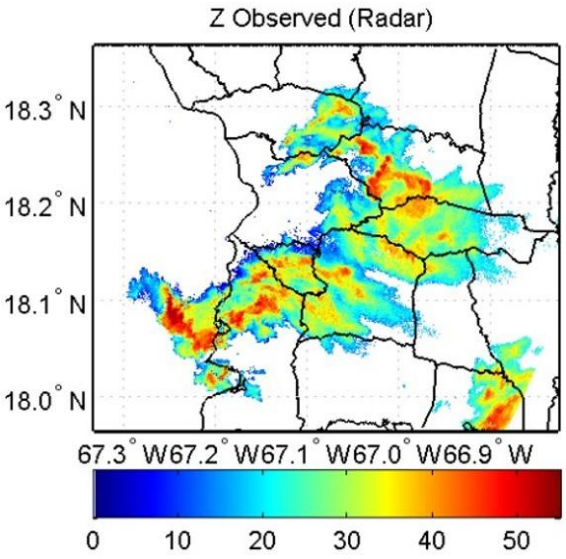

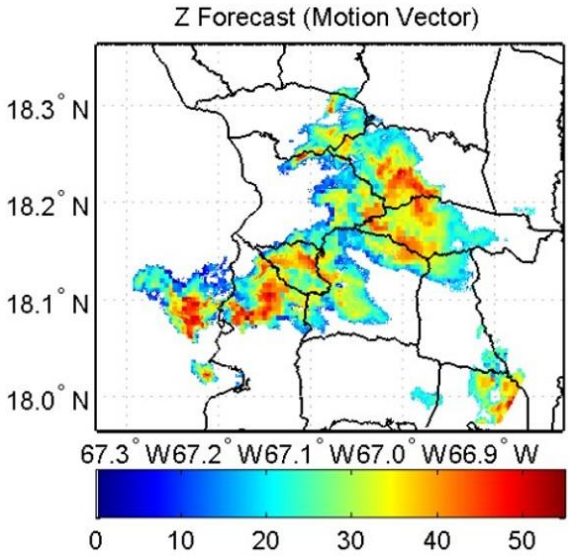

Figure 4. Top panel shows the observed rainfall and the bottom pane shows the forecast for a storm that occurred on Puerto Rico on March 28, 2012, 1840 UTC.

4. MODEL VALIDATION

Model validation consists of comparing the predicted values from the model with observations over the same time and space, and is presented for the five storms described in Table 1. The accuracy of rainfall predictions of each pixel can be measured by decomposing the rainfall process into sequences of discrete and continuous random variables, i.e., the presence or absence of rainfall events and rainfall intensity. The occurrence of rainfall events in a given area at a particular time follows a Bernoulli process and consequently, the prediction accuracy of rainfall events can be measured by analyzing the bivariate probability distribution of rain/no-rain events, which the bivariate distribution is usually estimated and presented as a contingency table (Wilks, 1995).

In this work, the rainfall estimated from radar reflectivity was considered as the observed rain/no rain stages and the estimated stages were the forecast values from our algorithm for lead times of 10, 20, and 30 minutes. The contingency tables associated with the five studied storms were computed (not shown). When the true stage coincides with the predicted stage, the event is declared a hit score; otherwise, it is considered a failure score. The

Corresponding author Nazario D. Ramirez-Beltran, Industrial Engineering, University of Puerto Rico, Mayaguez, P.R. 00680, Nazario.ramirez@upr.edu

percentage of hits in a given contingency table is called the hit rate (HR). The probability of detection (POD) and false alarm rate (FAR) scores include dichotomous yes/no forecast situation and a two-way table for each lead time was developed. A popular index (Wilks, 1995) that measure forecast accuracy is known as the Heidke Skill Scores (HSS). Essentially, HSS measures the fractional improvement of the forecast over the standard forecast. The range of the HSS is $-\infty$ to 1. Negative values indicate the worse forecast, 0 means no skill, and a perfect forecast obtains a HSS of 1. The Performance Index (PI) is introduced in this work to measure the overall dichotomous (rain/no rain) forecast accuracy of the model, and is computed as a function of HR, FAR and POD. The PI varies from 0 to 1, and a value of 1 corresponds to the best algorithm performance; whereas, 0 corresponds to the worse case. The PI is defined as follows:

$$\mathrm{PI} = 1 - \frac{FAR - POD - HR + 2}{3} \qquad (8)$$

Table 2 shows model performance scores for HR, POD, FAR, Discrete Bias (DB), HSS and PI. The studied storms provide an average HR of 0.89, 0.86, and 0.85 for lead times of 10, 20 and 30 minutes, respectively. The HR scores indicate that longer lead times reduced the HR. The POD of storm varies from 0.64, 0.53, 0.44 and the FAR from 0.27, 0.37, and 0.44 for lead times of 10, 20 and 30 minutes respectively. Figure 4 (top panel) shows POD and FAR, which should be analyzed simultaneously. It is expected that the POD approaches 1, while the FAR approaches 0 in the ideal situation. The model exhibits an underestimation since the average DB is 0.88, 0.83, and 0.79 for lead times of 10, 20, and 30 minutes, respectively. It can be noted that forecast skill degraded since the HSS is 0.61, 0.49, and 0.40 for lead times 10, 20, 30 min respectively. Figure 4 (bottom panel) shows the PI of 0.75, 0.67, and 0.61 for 10, 20, and 30 minutes lead times.

Table 2. Model accuracy scores

Forecast	10 minutes	20 minutes	30 minutes
HR	0.89	0.86	0.85
POD	0.64	0.53	0.44
FAR	0.27	0.37	0.44
DB	0.88	0.83	0.79
PI	0.75	0.67	0.61
HSS	0.61	0.49	0.40

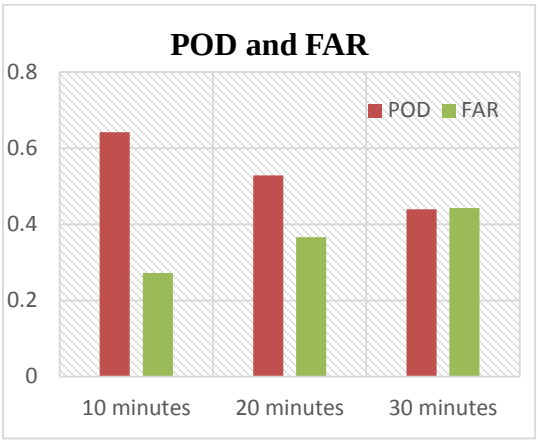

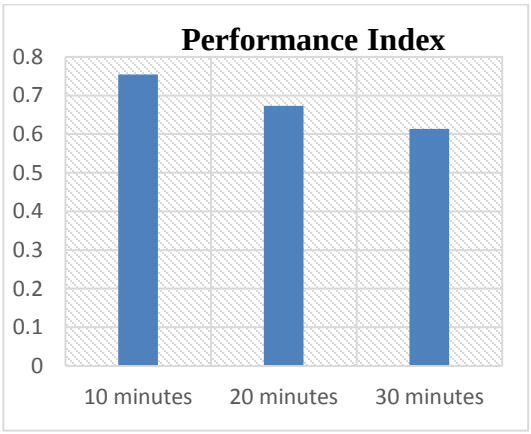

Figure 4. The top panel shows the probability of detection and the false alarm rate for the corresponding lead times. The bottom panel shows PI for different lead times.

The continuous validation strategy consists of comparing each pixel of the predicted rainfall intensity made at a given time and for a specific lead time with the corresponding observed rainfall intensity. Thus, the continuous accuracy scores used here were the root mean square error (RMSE) and the bias ratio (BR). The calculation of these scores are given as follows:

$$RMSE_{t+l} = \sqrt{\frac{\sum_{i=1}^{n}\sum_{j=1}^{m}[y_{t+l}(i,j) - \hat{y}_{t+l}(i,j)]^2}{nm}}, \quad l = 10, 20, 30 \qquad (9)$$

Corresponding author Nazario D. Ramirez-Beltran, Industrial Engineering, University of Puerto Rico, Mayaguez, P.R. 00680, Nazario.ramirez@upr.edu

$$\overline{RMSE}_l = \frac{\sum_{t=1}^{N} RMSE_{t+l}}{N}, \quad (10)$$

$$BR_{t+l} = \frac{\sum_{i=1}^{n}\sum_{j=1}^{m} \hat{y}_{t+l}(i,j)}{\sum_{i=1}^{n}\sum_{j=1}^{m} y_{t+l}(i,j)}, \quad (11)$$

$$\overline{BR}_l = \frac{\sum_{t=1}^{N} BR_{t+l}}{N}, \quad (12)$$

where $\hat{y}_{t+l}(i,j)$ is the predicted rainfall intensity made at time *t* with *l* lead time units for a pixel located at (i,j), and $y_{t+l}(i,j)$ is the corresponding observed rainfall intensity; *N* is the total number of units of time that rainfall was observed, *n* is the total number of rows and *m* is total number of columns of rainfall area. The RMSE and the BR for the five (5) studied events are given in Table 3, which also shows the corresponding average values. The average RMSE are 0.03, 0.08, and 0.16 mm and the average BR are 0.97, 0.97, and 0.94 for lead times 10, 20, and 30 minutes, respectively. The RMSE shows evidence that the prediction errors are degraded as soon as the lead time becomes larger. The RMSE is increasing due to the fact that larger errors are occurring as soon as the lead time is increasing.

Table 3. Average root mean square error and bias ratio

	10 minutes		20 minutes		30 minutes	
Rainfall Event	Average RMSE (mm)	Average BR	Average RMSE (mm)	Average BR	Average RMSE (mm)	Average BR
1	0.04	0.95	0.14	0.91	0.21	0.83
2	0.01	0.97	0.03	0.98	0.03	0.97
3	0.01	1.03	0.03	1.12	0.04	1.19
4	0.06	0.95	0.15	0.92	0.36	0.86
5	0.03	0.97	0.06	0.92	0.15	0.84
Average	**0.03**	**0.97**	**0.08**	**0.97**	**0.16**	**0.94**

Figure 5 shows the accumulation of rainfall for every pixel and during 7 hours of rainfall event that occurred in Puerto Rico in March 28, 2012. Upper panel shows TropiNet observed rainfall (mm) and bottom panel show the predicted rainfall (mm). The upper panel of Figure 6 shows the average rainfall for all rain pixels for each time interval (10 minutes) and during the entire rainfall event (March 28, 2012). The blue line represents the observed (TropiNet) data and the green line represents the predicted precipitation at 10 minutes lead time. The bottom panel of Figure 6 shows the rainfall accumulated for all rain pixels during 7 hours of a rainfall event (March 28, 2012).

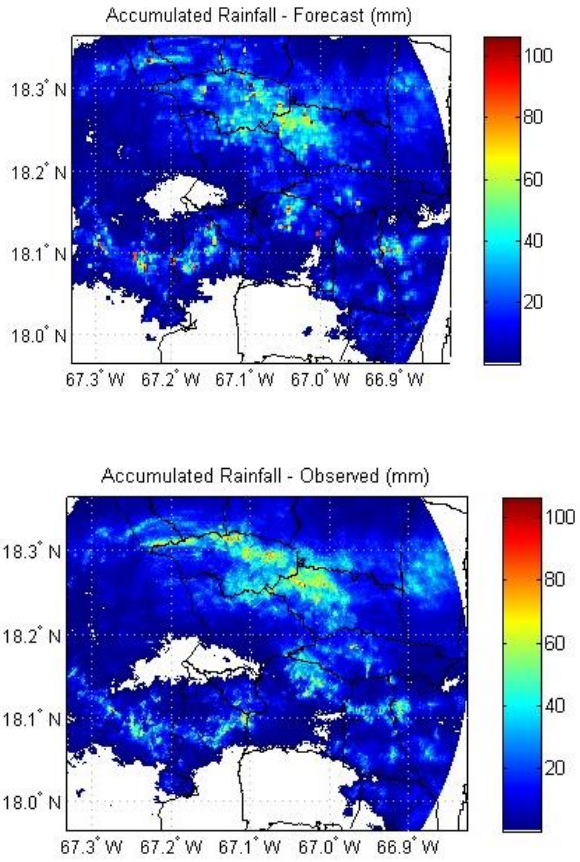

Figure 5. Rainfall accumulated during 7 hours for the event that occurred in Puerto Rico on March 28, 2012. Upper panel show the accumulated predicted rainfall (mm) for a 10 minutes lead time and bottom panel show TropiNet observed accumulated rainfall (mm).

Corresponding author Nazario D. Ramirez-Beltran, Industrial Engineering, University of Puerto Rico, Mayaguez, P.R. 00680, Nazario.ramirez@upr.edu

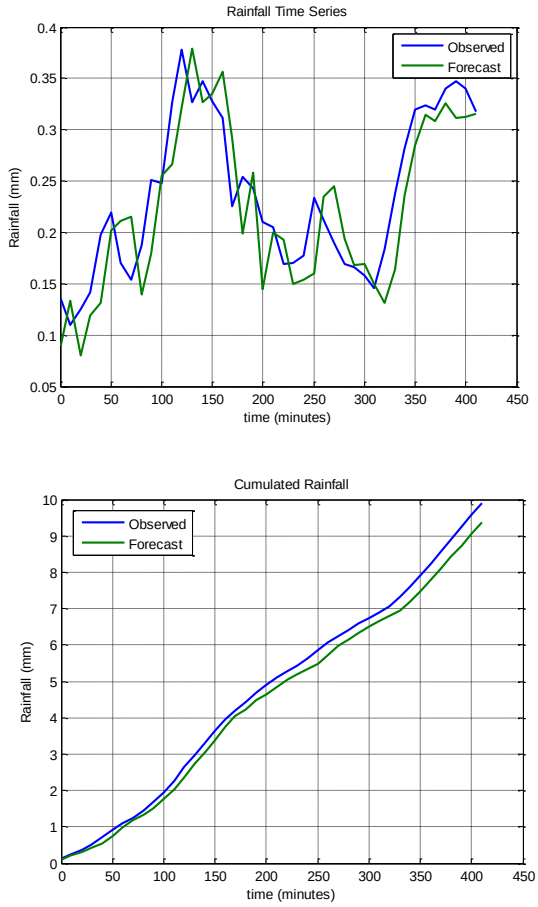

Figure 6. Top panel shows the average rainfall for all rain pixels during each time interval (10 minutes). The bottom panel shows the accumulated precipitation for all rain pixels during 7 hours of a rainfall event that occurred on March 28, 2012. The blue line represents the observed (TropiNet) data and the green line represents the forecasts at 10 minutes lead time.

5. CONCLUSION AND RECOMMENDATIOS

Estimation of rain rate at a given space and time requires consideration of the clouds status at the current time and also at consecutive previous points in time as well as the influence of the motion vector; i.e., a statistical model that depends only on current cloud conditions may be an incomplete representation of the rainfall process because the rain rate at the current time is the result of the evolution of microphysical processes that started several minutes earlier while the wind vector determines the possible places where rain drops may arrive to the surface. Therefore, a reasonable model to represent the rain rate was introduced. The major contribution of this research is the postulated model represents the spatial and temporal variation of rainfall rate. Different parameter estimation is developing at each spatial and temporal domain, and the stochastic behavior of rainfall intensity was represented by an exponential time and spatial lag model, which is an approximation of a stochastic transfer function.

The rainfall nowcasting algorithm uses consecutive images of weather radar to forecast rainfall rate. The algorithm searches for contiguous rain pixels and identifies rain cells in the last two radar images to estimate the cloud motion vector. The cloud motion vector is then used to estimate the most likely future locations of the rain pixels, and finally, nonlinear regression models are postulated to forecast the intensity of rainfall rate at each rain pixel. The proposed rainfall nowcasting algorithm was validate with five (5) storms with a total of 30 hours of precipitation and results show that the nowcasting algorithm is a potential tool to couple with a hydrological numerical model to predict the most likely inundations areas.

Puerto Rico is heavily affected by rainfall due to warm-top convective processes that are induced by local sea breeze- and/or orographic features and also by tropical storms and cold fronts. A ceilometer shows that some of the local convective storms developed in the western part of Puerto Rico are below 3 km; i.e., some storms are missed because NEXRAD radar is located about 104 km away from the studied area and reflectivity is measured at about 3 km above the surface because of the mountains. The use of a radar system with high resolution and covering the NEXRAD missing areas is important for flood forecasting and for understanding hydro meteorological processes. The current research represents the first time that a high resolution radar technology was used for rainfall forecasting

Corresponding author Nazario D. Ramirez-Beltran, Industrial Engineering, University of Puerto Rico, Mayaguez, P.R. 00680, Nazario.ramirez@upr.edu

and hydrological analyses in western Puerto Rico.

Acknowledgements

This work was supported primarily by National Science Foundation (NSF) Engineering Research Centers: Collaborative Adaptive Sensing of the Atmosphere: **(**ERC-CASA) under the grant AN0313747 and NSF MRI ECCS-0821331 "Development of a Meteorological Radar Network for Puerto Rico's West Coast of PR". The National Oceanic and Atmospheric Administration: Cooperative Remote Sensing Science and Technology Center (NOAA-CREST) also supported this research under grant NA11SEC4810004. Any opinions, findings, conclusions, or recommendations expressed in this material are those of the authors and do not necessarily reflect those of the NSF and/or NOAA.

References

Abraham, B., J. Ledolter. 1983. *Statistical Methods for Forecasting*, Wiley 445 pp.

Box, G.E.P., G.M. Jenkins, and G.C. Reinsel. 1994. *Time Series Analysis: Forecasting and Control*, third edition, Prentice-Hall International, Inc. pp 614.

Burroughs, W.J., 2001. *Climate Change: A Multidisciplinary Approach*. Cambridge University Press, United Kindom, pp 296.

Cowpertwait, P., V. Isham, and Ch. Onof. 2007. Point process models of rainfall: developments for fine-scale structure. *Proceedings of the Royal Society*, 463, 2569-2587.

Dixon, M., and G. Weiner. 1993. TITAN: Thunderstorm Identification, Tracking, Analysis, and Nowcasting---A Radar-based Methodology. *Journal of Atmospheric and Ocean Technology*, Vol. 10, No. 6. pp 785-997.

Galvez, M.B., J. G. Colom, V. Chandrasekar, F. Junyent, S. Cruz-Pol, R. A. Rodriguez Solis, L. Leon, J. J. Rosario-Colon, B. De Jesus, J. A. Ortiz, and K. M. Mora Navarro. First Observations of the Initial Radar Node in the Puerto Rico Tropinet X-Band Polarimetric Doppler Weather Testbed, *IGARSS,* 2013, 2337-2340.

Galvez, M. B., J. G. Colom, V. Chandrasekar, F. Junyent, S. Cruz-Pol, R. A. Rodriguez Solis, "Salient Features of the Radar Nodes in the Puerto Rico Tropical Weather Testbed," *IGARSS*, 2009.

Houze, R. A., Jr., 1993: *Cloud Dynamics*. Academic Press, San Diego, 573 pp.

Montgomery, D.C., E. A. Peck, and G. G. Vining. 2012. *Introduction to Linear Regression Analysis*. Fifth edition, John Wiley & Sons.

National Oceanic and Atmospheric Administration, and the National Weather Services (NOAA/NWS). 2014. Multisensor Precipitation Estimation and Nowcasting for Flash Floods http://www.nws.noaa.gov/oh/hrl/hag/empe_mpn/

Ramirez-Beltran, N.D, Castro, J.M., Harmsen, and E. Vasquez, R. (2008). Stochastic transfer function models and neural networks to estimate soil moisture. *Journal of the American Water Resources Association*. Vol. 44, No. 4, pp 847-865.

Ramirez-Beltran, N.D., J. M. Castro, and J. Gonzalez. (2005). An algorithm for predicting the spatial and temporal distribution of rainfall rate, *An International Journal of Water*. In press.

Rodriguez-Iturbe, I., V.K. Gupta, and E. Waymire. 1984. Scale Consideration in the Modeling of Temporal Rainfall. *Water Resources Research*, 20(11): 1611-1619.

Rodriguez-Iturbe, I., D.R. Cox, and V. Isham. 1987. Some Models for Rainfall Based on Stochastic Point Process, *Proc. R. Soc. London, Ser. A*., 410: 269-288.

Thorndahl, S., Rasmussen, M.R., Nielsen, J.E., and Larsen, J.B. Uncertainty on Nowcasting of radar rainfall- a case study of GUE methodology. *ERAD 2010 The sixth European Conference on Radar in Meteorology and Hydrology*. September 6 - 10, 2010, Sibiu, Romania.

Van Horne, M.P. *Short-Term Precipitation Nowcasting for Composite Radar Rainfall Fields*. Master thesis, in Civil and Environmental Engineering, Massachusetts Institute of Technology, September, 2003.

Corresponding author Nazario D. Ramirez-Beltran, Industrial Engineering, University of Puerto Rico, Mayaguez, P.R. 00680, Nazario.ramirez@upr.edu

Wilks, D.S., 1995: *Statistical Methods in the Atmospheric Sciences: An Introduction*. Academic Press, San Diego, 467 pp

Wilson, J.W., Precipitation Nowcasting: Past, present and future. *Sixth International Symposium on Hydrological Applications of \Weather Radar*. Melbourne, Australia, from 1-4 February 2004

Wackernagel, H. 2003. *Multivariate Geostatistics: An Introduction with Applications*. Springer, Third edition, France, pp 387.

Corresponding author Nazario D. Ramirez-Beltran, Industrial Engineering, University of Puerto Rico, Mayaguez, P.R. 00680, Nazario.ramirez@upr.edu